Coastal Engineering 67 (2012) 54–66

Contents lists available at SciVerse ScienceDirect

Coastal Engineering

journal homepage: www.elsevier.com/locate/coastaleng

A new approach to handle wave breaking in fully non-linear Boussinesq models

M. Tissier [a,*], P. Bonneton [a], F. Marche [b], F. Chazel [c], D. Lannes [d]

[a] Université Bordeaux 1, CNRS, UMR 5805-EPOC, Talence, F-33405, France
[b] I3M, Université de Montpellier 2, CC 051, F-34000, Montpellier, France
[c] Université de Toulouse, UPS/INSA, IMT, CNRS UMR 5219, F-31077 Toulouse, France
[d] DMA, Ecole Normale Supérieure et CNRS UMR 8553, 45 rue d'Ulm, F-75005, Paris, France

ARTICLE INFO

Article history:
Received 16 November 2011
Received in revised form 9 April 2012
Accepted 11 April 2012
Available online 14 May 2012

Keywords:
Finite volume
Breaking model
Shock theory
Fully non-linear Boussinesq model

ABSTRACT

In this paper, a new method to handle wave breaking in fully non-linear Boussinesq-type models is presented. The strategy developed to treat wave breaking is based on a reformulation of the set of governing equations (namely Serre Green–Naghdi equations) that allows us to split them into a hyperbolic part in the conservative form and a dispersive part. When a wave is ready to break, we switch locally from Serre Green–Naghdi equations to Non-linear Shallow Water equations by suppressing the dispersive terms in the vicinity of the wave front. Thus, the breaking wave front is handled as a shock by the Non-linear Shallow Water equations, and its energy dissipation is implicitly evaluated from the mathematical shock-wave theory. A simple methodology to characterize the wave fronts at each time step is first described, as well as appropriate criteria for the initiation and termination of breaking. Extensive validations using laboratory data are then presented, demonstrating the efficiency of our simple treatment for wave breaking.

1. Introduction

Non-linear wave transformations in shallow water, and associated processes such as wave-breaking and run-up, play a key role in the nearshore dynamics. A detailed knowledge of instantaneous non-linear wave characteristics is required in place of wave-averaged quantities for an accurate prediction of suspended sediment transport. Elgar et al. (2001) highlighted the importance of wave asymmetry for onshore bar migration, while recent studies focused on the influence of different combinations of wave skewness and asymmetry on the net sediment flux (Grasso et al., 2011; Ruessink et al., 2009). Non-linear effects are also responsible for the generation of infra-gravity waves, which can strongly affect beach and dune erosion during high energy events (Roelvink et al., 2009). An accurate description of non-linear wave transformations is also necessary for the study of coastal flooding due to storm waves or tsunamis. The description of these highly non-linear and unsteady processes requires phase-resolving models with a good description of breaking and run-up over complex bathymetries. The most accurate models for the description of wave breaking are based on the Navier–Stokes equations. They can give a detailed description of wave breaking, including wave overturning, but are highly computationally demanding and therefore not suitable for large scale propagation applications. For this reason, phase-resolving models based on depth-averaged equations are still an attractive way to describe wave transformation in the nearshore zone. Two kinds of approaches can be considered: the models can be based on Non-linear Shallow Water (NSW) or Boussinesq-type (BT) equations.

NSW models, with the help of shock-capturing schemes, can accurately reproduce broken wave dissipation and swash oscillations without any ad hoc parametrization (Bonneton, 2007; Brocchini and Dodd, 2008; Kobayashi et al., 1989; Marche et al., 2007). The absence of dispersive effects restricts their validity domain to areas where non-linearities predominate, such as the inner surf and swash zones. They are in particular not valid in the shoaling zone, since the absence of dispersive effects would lead to an incorrect prediction of the location of wave breaking. On the other hand, BT equations take into account at different degrees of accuracy both non-linear and dispersive aspects of wave propagation. Denoting by a the order of free-surface amplitude, h_0 the characteristic water depth and L the characteristic horizontal scale, most of Boussinesq models used for nearshore applications are based on a classical shallow water assumption $\mu=(h_0/L)^2\ll 1$ and balance between dispersion and non-linearity $\varepsilon=O(\mu)\ll 1$,with $\varepsilon=a/h_0$. Yet, these assumptions do not always hold in the nearshore, in particular in the final stages of shoaling and in the surf and swash zones, where ε can be of order 1. For such applications, fully non-linear BT equations are required. Wei et al. (1995) showed that accounting for strong non-linearities in BT approaches leads to significantly improved predictions

* Corresponding author. Now at Institute for Marine and Atmospheric Research, Department of Physical Geography, Faculty of Geosciences, Utrecht University, P.O. Box 80115, 3508 TC, Utrecht, The Netherlands. Tel.: +31 3 02 53 74 53; fax: +31 3 02 53 11 45.
E-mail addresses: M.F.S.Tissier@uu.nl (M. Tissier), p.bonneton@epoc.u-bordeaux1.fr (P. Bonneton), fabien.marche@math.univ-montp2.fr (F. Marche), florent.chazel@math.univ-toulouse.fr (F. Chazel), david.lannes@ens.fr (D. Lannes).

0378-3839/$ – see front matter © 2012 Elsevier B.V. All rights reserved.
doi:10.1016/j.coastaleng.2012.04.004

of wave heights, wave celerities and internal kinematics prior to breaking. The first set of fully non-linear BT equations was derived by Serre (1953), and extended to the 2D case by Green and Naghdi (1976). These equations, called Serre Green–Naghdi (S–GN) equations thereafter, are now recognized to be the relevant system to describe fully non-linear weakly dispersive waves propagating in the nearshore (Lannes and Bonneton, 2009). They can accurately predict most phenomena exhibited by non-breaking waves in finite depth. However, as they do not include intrinsically energy dissipation due to wave breaking, they become invalid in the surf zone. Besides, S–GN dispersive terms become nonphysical in the vicinity of the breaking wave fronts. Several attempts have been made to introduce wave breaking in BT models by the mean of *ad hoc* techniques (e.g., Cienfuegos et al., 2010; Kennedy et al., 2000; Madsen et al., 1997). These approaches generally require (1) the inclusion of an energy dissipation mechanism through the activation of extra terms in the governing equations when wave breaking is likely to occur; (2) explicit criteria to activate/deactivate these extra terms; (3) a method to follow the waves during their propagation since the breaking parametrizations depend on the age of the breaker. Moreover, the breaking model parameters need to be calibrated to ensure that the artificially induced energy dissipation is in agreement with the rate of energy dissipated in surf zone waves. FUNWAVE (Kirby et al., 1998) is a well-known example of this kind of models. It is based on the fully non linear Boussinesq equations of Wei et al. (1995), with additional parametrizations to include wave breaking and run-up (Kennedy et al., 2000). Except for being formulated in terms of the velocity vector at an arbitrary z level, the equations of Wei et al. are equivalent to the S–GN equations.[1] FUNWAVE gives a very good description of wave transformations in the nearshore, but each use of the model implies the tuning of several parameters, as the ones determining wave-breaking dissipation and run-up (Bruno et al., 2009). Recently, Cienfuegos et al. (2010) showed that Kennedy et al.'s eddy viscosity breaking model could hardly predict simultaneously accurate wave height and asymmetry along the surf zone. This observation motivated the development of a new 1D wave-breaking parametrization including viscous-like effects on both the mass and the momentum equations. This approach is able to reproduce wave height decay and intraphase non-linear properties within the entire surf zone (Cienfuegos et al., 2010). However, the extension of this parametrization to 2D wave cases remains a very difficult task. Therefore, alternative approaches to handle wave breaking in BT models may prove very useful.

Recently, the so-called non-hydrostatic models, governed by the NSW equations including non-hydrostatic pressure, have been introduced as an alternative to BT models[2] (e.g., Zijlema et al., 2011). They can be run in multi-layered mode, improving their frequency dispersion properties, but also include a special treatment for wave breaking (classical Prandlt mixing length parametrization) as they do not explicitly account for small-scale turbulent processes.

The fully non-linear numerical model presented in this study is based on S–GN equations. It is worthwhile to note that S–GN equations degenerate naturally into NSW equations when dispersive effects are negligible. These equations are therefore well-suited to describe wave propagation until the swash zone. In order to treat wave breaking, a hybrid approach has been developed. S–GN equations are reformulated in a way that allows us to split them into a hyperbolic part corresponding to the NSW equations in the conservative form and a dispersive part (see Bonneton et al., 2011b). The idea is to switch from S–GN to NSW equations when the wave is ready to break by suppressing the dispersive term. This method allows for a natural treatment of wave breaking, since the energy dissipation due to wave breaking is predicted implicitly by the shock theory, and does not require to be parametrized. It is an important point since the amount of energy dissipated will determine crucial phenomena such as the water level set-up (Bonneton, 2007), and will impact wave-driven circulation (Bonneton et al., 2010; Bühler, 2000; Smith, 2006).

From a numerical point of view, an operator-splitting approach with hybrid finite volume/finite-difference schemes has been implemented (Bonneton et al., 2011b), allowing for the most effective schemes to be used for each part of the equations. Some hybrid numerical methods have already been developed in the past years, mainly within the framework of weakly non-linear BT equations (Briganti et al., 2004; Erduran, 2007; Erduran et al., 2005; Orszaghova et al., 2012; Shiach and Mingham, 2009; Soares-Frazão and Guinot, 2008; Soares-Frazão and Zech, 2002; Tonelli and Petti, 2009, 2010, 2012; Weston et al., 2003), but also recently within the framework of fully-non-linear BT models (Shi et al., 2012). Among these models, only few take advantage of the shock-capturing properties of the Finite Volume schemes to treat wave breaking (Orszaghova et al., 2012; Shi et al., 2012; Tonelli and Petti, 2009, 2010, 2012; Weston et al., 2003). A natural approach to handle wave breaking with this kind of models is to estimate the breaking point location and subsequently divide the numerical domain spatially into pre- and post- breaking areas, respectively governed by BT and NSW equations (e.g. Shi et al., 2012; Tonelli and Petti, 2009, 2010; Weston et al., 2003). This simple decomposition is of great interest for engineering purposes, in particular for the study of submersion risks, traditionally based on NSW models. Indeed, it allows for an accurate and simple description of both non-breaking and breaking wave transformations, and a treatment of shoreline motions without any parametrization. However, most of these models do not include an explicit criterion for the termination of breaking. Applying these methods to the description of irregular wave trains propagating over uneven bathymetries is therefore not straightforward, since in this case, series of alternatively breaking and non-breaking waves can be observed at a given time. It is only recently that Tonelli and Petti (2012) applied an extended version of their hybrid model (including an additional criterion for the switch back to BT equations) to describe the transformation of irregular waves.

In this paper, a new approach to handle wave breaking in hybrid models is presented. Instead of defining extended breaking areas where the flow is governed by the NSW equations, we treat individually the breaking of each wave front. More precisely, our breaking model is based on switches performed locally in space and time from S–GN to NSW equations in the vicinity of the wave fronts. With this local treatment, we intend to obtain a model able to account simultaneously and accurately for the effects of dispersion, non-linearities and wave breaking for a given wave. This is of importance when considering for instance tsunami wave front transformations in the nearshore, which can evolve into a large range of bore types, including partially breaking undular bores. Moreover, the proposed "wave-by-wave" treatment allows for a precise description of the breaking events, from the initiation to the termination. The approach is therefore

[1] It is shown in Lannes and Bonneton (2009) that the Green–Naghdi Eqs. (1) and (2) are the same, written in a different form, as the equations derived in Green and Naghdi (1976) and Miles and Salmon (1985). In Wei et al. (1995), the velocity unknown is not the averaged velocity u but, as in Nwogu (1993), the velocity taken at one arbitrary depth $z_\alpha(t,x)$, denoted by $V_\alpha(t,x)=V(t,x,z_\alpha(t,x))$. Replacing u in (1)–(2) by its expression in terms of V_α yields the same equations as in Wei et al. (1995), up to $O(\mu^2)$ terms. We refer to Section 2 of Chazel et al. (2010) for more details on this point.

[2] However, the model derived in Zijlema et al. (2011) in its one-layer formulation (Eqs. (18)–(21)) can be rewritten in a quasi BT form:

$$\partial_t\zeta+\partial_x(hu)=0$$
$$\partial_t u+u\partial_x u+g\partial_x\zeta=\frac{1}{4h}\left[\partial_x\left(h^3\partial_{xt}u\right)-\partial_x\left(h^2\partial_x(hu)\partial_x u\right)\right],$$

where several non-linear terms present in the S–GN equations have been neglected; moreover, the linear wave celerity associated to these equations is given by $c^2=gh_0(1-\mu/4)$ which differs at order $O(\mu)$ from the exact linear wave celerity $c^2=gh_0\frac{\tanh(\mu^{1/2})}{\mu^{1/2}}$, while for standard Boussinesq models one gets $c^2=gh_0(1-\mu/3+O(\mu^2))$, which is correct up to $O(\mu^2)$ terms. The precision of these models, that is, the error between the solution of the Green–Naghdi equations and the solution of the full Euler equations is then of order $O(\mu^2 t)$, as shown in Alvarez-Samaniego and Lannes (2008).

well-suited to describe the transformation of irregular wave trains, as well as their transformations over complex bathymetries, including barred beaches.

The numerical model is briefly described in Section 2. The strategy developed to handle wave breaking is then presented in Section 3. Extensive validations using experimental data are then performed (Section 4), including periodic wave transformations over a planar beach, solitary wave breaking, run-up and overtopping, and wave breaking over a bar. At last, some preliminary tests concerning hydraulic bore dynamics are performed, showing promising results concerning the model ability to predict the complex transition from undular to breaking bore.

2. Description of the model

Our model is based on a new 2D conservative S–GN formulation. These equations and the numerical methods to solve them are described in Bonneton et al. (2011b). In this section we sum up the main characteristics of our S–GN model in 1D.

2.1. Governing equations

The model is based on the S–GN equations. These equations can be formulated in term of the conservative variables (h, hu) in the following dimensionalized form:

$$\begin{cases} \partial_t h + \partial_x(hu) = 0, \\ \partial_t(hu) + \partial_x\left(hu^2 + gh^2/2\right) = -gh\partial_x b + \mathcal{D} - f\dfrac{1}{h}\|u\|u, \end{cases} \tag{1}$$

with u the depth-averaged horizontal velocity, ζ the surface elevation, h the water depth, b the variation of the bottom topography and f a non-dimensional friction coefficient. $\mathcal{D}$ characterizes non-hydrostatic and dispersive effects and writes:

$$\mathcal{D} = \frac{1}{\alpha}gh\partial_x\zeta - \left(1 + \alpha h\mathcal{T}\frac{1}{h}\right)^{-1}\left[\frac{1}{\alpha}gh\partial_x\zeta + h\mathcal{Q}_1(u)\right], \tag{2}$$

where the linear operator $\mathcal{T}$ is defined as

$$\mathcal{T}w = -\frac{h^2}{3}\partial_x^2 w - h\partial_x h\partial_x w + \left(\partial_x\zeta\partial_x b + \frac{h}{2}\partial_x^2 b\right)w, \tag{3}$$

and:

$$\begin{aligned}\mathcal{Q}_1(u) = {} & 2h\partial_x\left(h + \frac{b}{2}\right)(\partial_x u)^2 + \frac{4}{3}h^2\partial_x u\partial_x^2 u + h\partial_x^2 bu\partial_x u \\ & + \left(\partial_x\zeta\partial_x^2 b + \frac{h}{2}\partial_x^3 b\right)u^2.\end{aligned} \tag{4}$$

α is an optimization parameter that should be taken equal to 1.159 in order to minimize the phase and group velocity errors in comparison with the linear Stokes theory (see the dispersion correction method discussed in Cienfuegos et al. (2006)). Note that the range of validity of this set of equations can been extended to deeper water, using some additional optimization parameters, as described in Chazel et al. (2010).

The proposed formulation has two important advantages. First of all, the dispersive term does not require the direct computation of any third order derivative, allowing for more robust numerical computations. Moreover, if $\mathcal{D}=0$, we obtain the NSW equations in their conservative form. The formulation is therefore well-suited for a splitting approach separating the hyperbolic and the dispersive part of the equations, allowing for an easy coupling of the sets of equations.

2.2. Numerical methods

At each time step δ_t, we decompose the solution operator $S(\cdot)$ associated to Eq. (1) by the second order splitting scheme

$$S(\delta_t) = S_1(\delta_t/2)S_2(\delta_t)S_1(\delta_t/2), \tag{5}$$

where S_1 and S_2 are respectively associated to the hyperbolic and dispersive parts of the S–GN Eq. (1). More precisely:

- $S_1\ (t)$ is the solution operator associated to NSW equations

$$\begin{cases} \partial_t h + \partial_x(hu) &= 0, \\ \partial_t(hu) + \partial_x\left(hu^2 + gh^2/2\right) &= -gh\partial_x b - f\dfrac{1}{h}\|u\|u. \end{cases} \tag{6}$$

- $S_2\ (t)$ is the solution operator associated to the remaining (dispersive) part of the equations,

$$\begin{cases} \partial_t h &= 0, \\ \partial_t(hu) &= \mathcal{D}. \end{cases} \tag{7}$$

2.2.1. Hyperbolic part

Our S–GN model has been developed as an extension of the widely validated NSW code SURF-WB (see Berthon and Marche, 2008; Marche et al., 2007). The system (6) can be regarded as a hyperbolic system of conservation laws with a topography source term and a friction term. To perform numerical approximations of the weak solutions of this system, we use high-order finite volume method in conservative variables, based on a positive preserving relaxation scheme and MUSCL reconstructions (see Berthon and Marche (2008)). Since we aim at computing the complex interactions between propagating waves and topography, including the preservation of motionless steady states, a well-balanced scheme is used for the discretization of the topography source term (see Audusse et al., 2004). Gathering these approaches, we obtain a high-order positive preserving well-balanced shock-capturing scheme, able to handle breaking bores propagation as well as moving shorelines without any tracking method (Marche et al., 2007). The friction term is treated following the method presented in Berthon et al. (2011).

2.2.2. Dispersive terms

System (7) is solved at each time step using a classic fourth-order finite-difference approach. It is worth mentioning that we only need to solve one *scalar* equation (rather than a set of two equations) during this dispersive step. Indeed, h remains constant owing to the first equation of (7).

Concerning the time discretization, explicit methods are used both in (S_1) and (S_2). The systems are integrated in time using a classical fourth-order Runge–Kutta method.

2.2.3. Treatment of the shoreline

No special tracking procedure is used to handle shoreline motions. Dry cells are defined as those in which the water depth is less than a threshold value h_ε. A small routine is applied to ensure the stability of the numerical results at the shoreline: when the water depth h is smaller than h_ε, we impose $v=0$ ($h_\varepsilon = 10^{-5}$ in Section 4). The dispersive terms are suppressed when the water depth vanishes.

Extensive validations of the numerical methods for the 1D problem can be found in Bonneton et al. (2011a,b) and Chazel et al. (2010).

3. Wave breaking

Prior to breaking, S–GN equations give a very accurate description of wave transformations, including internal kinematics (Carter and Cienfuegos, 2011). However, depth-averaged approaches cannot

reproduce wave overturning and small-scale processes related to wave breaking. Approximate representations of the breaking processes are therefore needed. They are generally less accurate in the first stages of breaking, in particular for plunging breakers. By switching locally to NSW equations, we decide to represent breaking wave fronts as shocks: we conserve mass and momentum across the wave front, and allow energy to dissipate, according to the shock theory. The switch from the S–GN to the NSW equations is performed locally in time and space, by skipping the dispersive step S_2 (δ_t) when the wave is ready to break. As we aim at applying our code to realistic incoming waves, implying different locations of the breaking point, we need to handle each wave individually. We present in this section a simple way to characterize the wave fronts at each time step, as well as adequate criteria for the initiation and termination of breaking.

3.1. Characterization of the wave fronts

The switches from one set of equations to another are performed in the vicinity of the wave fronts, defined as the parts of the waves lying between the crest and the trough in their direction of propagation. We therefore first need to locate the wave fronts of interest, that is to say the breaking or broken fronts as well as those likely to break, and then decide which set of governing equations should be applied in their vicinities.

A simple way to identify these wave fronts at each time step is to detect the shocks forming during the NSW steps through the study of the energy dissipation. Indeed, the energy dissipation forms peaks at the steepest parts of the wave fronts when shocks are forming. This method can also be applied to the detection of the wave fronts likely to break since shocks are already forming during the NSW steps at the last stages of shoaling. However, as long as the dispersive terms are activated, the dispersive step (S_2) counteracts the shock development occurring during the NSW steps (S_1), preventing wave breaking.

From a practical point of view, we compute at each time step the local energy dissipation $D(x, t)$ corresponding to the first NSW step:

$$D(x,t) = -(\partial_t \mathcal{E} + \partial_x \mathcal{F}), \tag{8}$$

with $\mathcal{E} = \frac{\rho}{2}\left(hu^2 + g\zeta^2\right)$ the energy density and $\mathcal{F} = \rho hu\left(\frac{u^2}{2} + g\zeta\right)$ the energy flux density. We then detect the local maxima of the dissipation, and consider that the wave fronts are centered on these peaks.

In order to distinguish broken wave fronts from others, we quantify the amount of energy dissipated at the wave front during the first NSW step (S_1). $D(x, t)$ is integrated over the front and normalized by the theoretical dissipation across a shock, defined as follows (Stocker, 1957):

$$D_b = \frac{\rho g}{4}\left(\frac{g(h_2+h_1)}{2h_1h_2}\right)^{1/2}(h_2-h_1)^3, \tag{9}$$

with h_1 and h_2 the water depth in front and behind the shock (see Fig. 1). h_1 and h_2 are respectively approximated by the water depth at the trough and the crest of the wave, defined as the closest surface elevation extrema to the dissipation peak. The normalized dissipation $\Gamma = \int_{front} D(x,t)dx/D_b$ is close to one for fully broken waves, close to zero when the wave is not breaking. Intermediate values can be found at the initiation and termination of breaking, i.e. when the breaker is not saturated ($(h_2-h_1)<H$, with H the wave height).

Thus, the study of Γ allows for a simple estimation of the wave "state" at each time step, without requiring any wave tracking technique. We consider that for $\Gamma \geq 0.5$, the wave is broken, and for $\Gamma < 0.5$, the wave is either non-breaking or at the very first stages of breaking. Additional criteria are needed to determine when to initiate/terminate wave breaking.

3.2. Breaking criteria

Several criteria for the initiation of breaking can be found in the literature (e.g., Bjørkavåg and Kalisch, 2011; Kennedy et al., 2000; Okamoto and Basco, 2006; Schäffer et al., 1993; Zelt, 1991). For the test cases presented in Section 4, a criterion based on the critical front slope (Schäffer et al., 1993) is applied, following Lynett (2006) which identified it as the least sensitive breaking threshold. We define Φ the maximal local front slope and Φ_i the critical slope, and for $\Phi \geq \Phi_i$ the breaking process starts. For our model with improved dispersive properties ($\alpha = 1.159$), we choose $\Phi_i = 30°$, optimal angle determined by Cienfuegos et al. (2010) for their S–GN model.

After breaking, the wave fronts are handled as shocks by the NSW equations. As long as they are governed by these equations, the shocks keep dissipating energy. A physical criterion is needed to determine when the switch back to S–GN equations has to be performed, allowing for the breaking process to stop. The proposed criterion is based on the analogy between a broken wave and a bore in the sense of a simple transition between two uniform levels (Peregrine, 1983). Bores stop breaking when their Froude number $Fr_1 = (c_b - u_1)/(gh_1)^{1/2}$, with c_b the bore celerity and u_1 the depth-averaged velocity in front of the bore, drops below a critical value Fr_c. Our criterion for the cessation of breaking is therefore the following: the wave stops breaking if $Fr_1 < Fr_c$, with Fr_1 rewritten as a function of h_1 and h_2 only using the mass and momentum conservation across the bore:

$$Fr_1 = \sqrt{\frac{(2h_2/h_1+1)^2-1}{8}}. \tag{10}$$

Experimental studies found that the Froude number at the cessation of breaking for a bore propagating on a flat rectangular channel was ranging from 1.2 to 1.3 (Chanson, 2008; Favre, 1935; Treske, 1994). In the following test cases, we set $Fr_c = 1.3$.

3.3. Suppression of the dispersive term

The zone over which we switch to NSW equations for a given wave is centered on the wave front, as illustrated in Fig. 1. Its horizontal length l_{NSW} must be larger than the order of magnitude of the physical length of the roller l_r ($l_{NSW} = a\ l_r$, $a > 1$) in order to avoid the nonphysical effects of the dispersive terms in the vicinity of the breaking wave front. Haller and Catalán (2010) found experimentally that $l_r \approx 2.9\ H$ was a good estimation of the roller length for well-

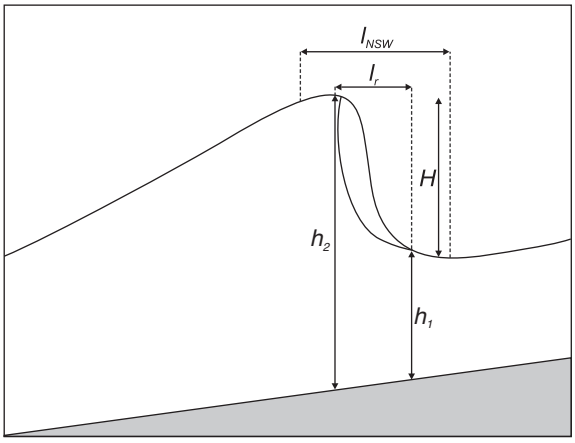

Fig. 1. Definition sketch for a broken wave propagating over a sloping beach. l_r: roller length. $l_{NSW} = 2.5 l_r$: width of the spatial zone where the switch from S–GN to NSW equations is performed.

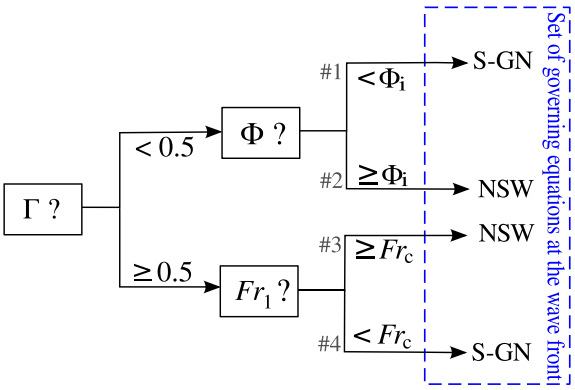

Fig. 2. Wave breaking model.

established breakers in agreement with previous experiments by Duncan (1981). Numerical tests showed that $a \approx 2.5$ was an appropriate value. Of note, the length l_{NSW} does not determine the amount of energy dissipated at the breaking wave front nor its spatial distribution. For this reason, model predictions appear to be weakly dependant from its value, as long as $l_{NSW} > l_r$.

The methodology to handle wave breaking is summarized in Fig. 2. At each time step, the wave fronts are first located and their normalized dissipation computed following the method detailed in Section 3.1. Four cases are then possible:

- If $\Gamma < 0.5$ and $\Phi < \Phi_i$: the wave is not breaking. The flow is governed by the S–GN equations (see Fig. 2, case 1).
- If $\Gamma < 0.5$ and $\Phi \geq \Phi_i$: the wave is in the first stages of breaking. The front is governed by NSW equations allowing the shocks to develop (case 2).
- If $\Gamma \geq 0.5$ and $Fr_1 \geq Fr_c$: the wave is broken. The wave front is locally governed by the NSW equations (case 3).
- If $\Gamma \geq 0.5$ and $Fr_1 < Fr_c$: the wave stops breaking. The wave front is governed by the S–GN equations (case 4).

Fig. 3 illustrates our wave-by-wave treatment of breaking using a simulation corresponding to Cox (1995) regular wave experiments. In the shoaling zone, the wave fronts are characterized by a normalized dissipation Γ close to zero. As they propagate shoreward, the waves gradually steepen. When their front slope reaches the critical value Φ_i, the switch to NSW equations is performed. The waves enter a transitional zone, where the fronts are steepening further while shocks are developing (case 2). After a while, the waves are fully broken, and their normalized dissipation is close to one (case 3). They dissipate their energy while propagating shoreward, leading to a progressive decrease of the breaker heights and front slopes. The waves will keep breaking as long as their Froude number is such as $Fr_1 \geq Fr_c$, i.e. until the shoreline in this case (see vertical lines in Fig. 3). If the broken waves were propagating over a trough (see §4.4 for instance), the bore Froude number would decrease and eventually get smaller than Fr_c. The switch back to S–GN equations would then be performed (case 4), resulting in the gradual disappearance of the shocks and the decrease of the normalized dissipation Γ.

The transition between the two systems is performed abruptly, without any smooth transition zone. In this way, wave propagation is governed by one given set of equations in each cell, and not by a nonphysical mix of both sets. The transition generates some disturbances, but they remain of small amplitude and do not lead to instabilities. No numerical filtering is applied. It is worth noting that the generation of oscillations is also observed for Boussinesq models based on the surface roller method when the extra terms responsible for wave breaking are activated.

The proposed breaking model has several advantages. First, the energy dissipation due to wave breaking is implicitly predicted by the shock theory and does not require to be parametrized contrary to most of the BT models. Moreover, the characterization of the waves at each time step is performed in a simple way through the study of the energy dissipation. The only important parameters to prescribe are the criteria for the initiation and termination of breaking. It is worth noting that the test cases presented in Section 4 were all simulated with the same set of parameters ($\Phi_i = 30°$, $Fr_c = 1.3$). The optimization parameter α for the dispersive properties is taken equal to 1.159.

4. Validations

In order to validate our model, classical test cases are first used. They involve the transformations of regular wave trains (Section 4.1) and solitary waves (Section 4.2) over sloping beaches. These commonly-used benchmarks allow for a rigorous testing of our breaking model. More challenging test cases are then considered. The ability of our model to describe wave breaking and swash motions over complex bathymetries, involving the water mass separation into disjoint water bodies is first studied (Section 4.3). We then investigate the model ability to predict wave transformations over a bar (Section 4.4). In this test case, a special focus is placed on the prediction of the termination of breaking and subsequent wave transformations after the bar. Bore dynamics for different Froude numbers is then studied (Section 4.5). These preliminary tests aim at investigating the model ability to account simultaneously for the effects of dispersion, non-linearities and wave breaking for a given wave.

4.1. Shoaling and breaking of regular waves over a sloping beach

4.1.1. Cox (1995)'s experiment

In our first test case we consider Cox (1995)'s regular waves experiment. Cnoidal waves of relative amplitude $H/h_0 = 0.29$ and period

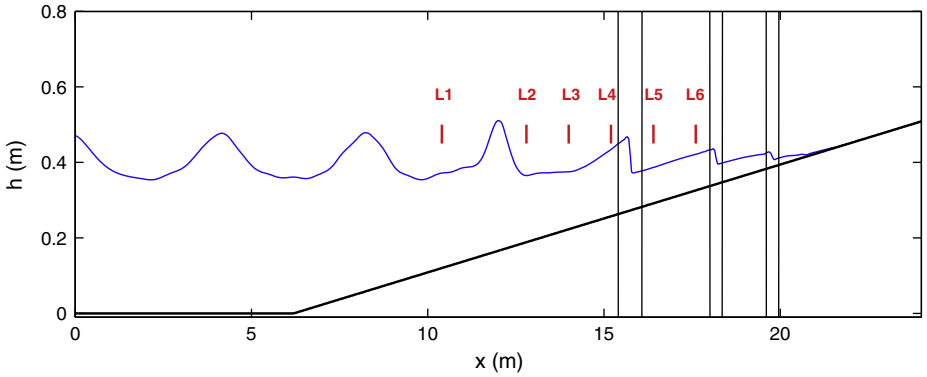

Fig. 3. Spatial snapshot of cnoidal waves propagating over a 1:35 sloping beach (Cox, 1995). L1 to L6: locations of the wave gauges. Between 2 consecutive vertical lines, the flow is governed by NSW equations.

$T=2.2$ s were generated in the horizontal part of a wave flume of depth $h_0=0.4$ m. They were then propagating and breaking over a 1:35 sloping beach. For this test case, synchronized time series of free-surface elevation are available at six locations, corresponding to wave gages located outside (L1 and L2) and inside (L3 to L6) the surf zone (see Fig. 3). During the experiment, waves were breaking slightly shoreward to L2.

For this simulation, we choose $\delta_x=0.04$ m, $\delta_t=0.01$ s. Fig. 3 shows a spatial snapshot of the free-surface profile computed with the model. It shows that the model is able to reproduce the typical saw-tooth profile in the Inner Surf Zone (ISZ). Fig. 4 compares the experimental and numerical time series of free-surface elevation for this experiment. We can see that we have a good overall agreement in both the shoaling and surf zones. The main discrepancies are observed in the vicinity of the breaking point, where the maximum wave height is underestimated. We can also notice that the numerical broken wave fronts are a bit too steep: this aspect will be discussed later in this section. It is worth noting that the time series are in phase for most of the wave gauges, demonstrating that wave celerity is well predicted by the model. The short time lag observed at the most onshore location (L6) is a consequence of the slight underestimation of the computed wave height in the inner surf zone (see also Fig. 5a, plain lines).

In particular, the model ability to describe non-linear wave shape is assessed through the computation of the crest-trough asymmetry or wave skewness parameter, *Sk*, and the left-right asymmetry parameter, *As*, defined as (Kennedy et al., 2000):

$$Sk=\frac{\left\langle\left(\zeta-\bar{\zeta}\right)^3\right\rangle}{\left\langle\left(\zeta-\bar{\zeta}\right)^2\right\rangle^{3/2}} \tag{11}$$

$$As=-\frac{\left\langle\mathcal{H}\left(\zeta-\bar{\zeta}\right)^3\right\rangle}{\left\langle\left(\zeta-\bar{\zeta}\right)^2\right\rangle^{3/2}}, \tag{12}$$

where $\bar{\zeta}$ is the wave-averaged surface elevation, $\langle\rangle$ the time-averaging operator and $\mathcal{H}$ the Hilbert transform.

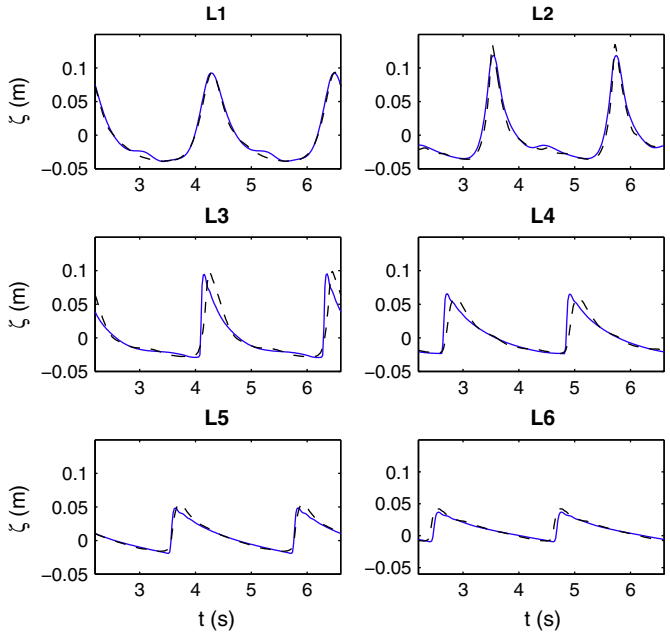

Fig. 4. Comparisons of computed (solid lines) and experimental (dashed lines) synchronized time series of free-surface elevation at the wave gauges for Cox (1995) breaking experiment ($\delta_x=0.04$ m and $\delta_t=0.01$ s).

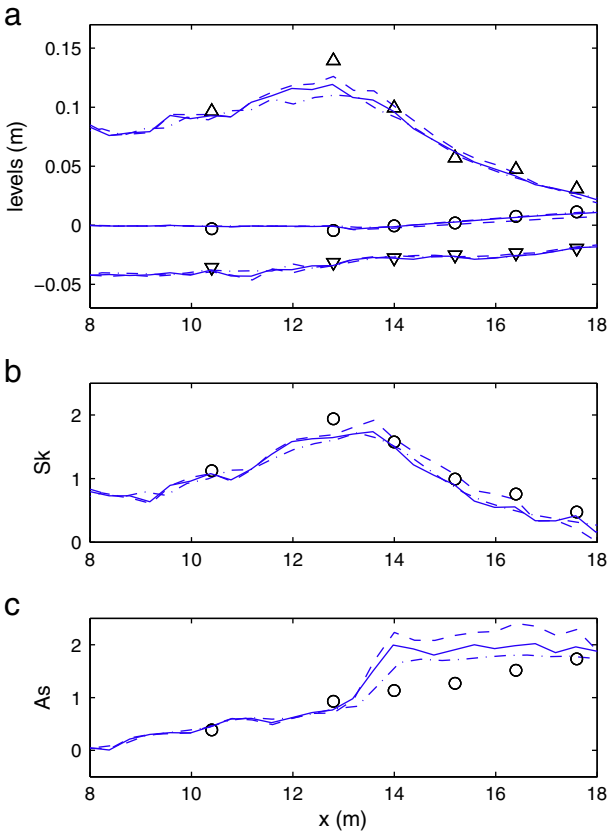

Fig. 5. Spatial evolution of computed (lines) and experimental data (symbols) for Cox (1995) experiments. (a) ○: Mean Water Level; ▽: trough elevation relative to MWL; △: crest elevation relative to MWL; (b) Wave skewness *Sk*; (c) Wave asymmetry *As*. The computations have been performed for different grid sizes: $\delta_x=0.04$ m (solid lines), $\delta_x=0.02$ m (dashed lines) and $\delta_x=0.06$ m (dash-dot lines).

It is well-known that once the waves are broken and represented as shocks, the front steepness depends on the spatial resolution δ_x. In order to evaluate how the grid spacing affects the model predictions, the numerical results obtained for two additional grid sizes are also displayed in Fig. 5 ($\delta_x=0.02$ m and 0.06 m, with $\delta_t=0.01$ s for all the computations). Fig. 5a shows that all the simulations underestimate the wave height at breaking, but predict similar locations of the breaking point, in agreement with the experimental data. It can be observed that the maximal wave crest elevation before breaking increases while the grid size decreases, leading to differences in the wave height predictions in the first stages of breaking. These differences result from the larger numerical dissipation for the simulations performed with the coarser grids, and are therefore not due to the shock-capturing properties of our model (see also Shi et al. (2012) for similar conclusions using their fully non-linear BT hybrid model). We can moreover see that the agreement between data and model is good concerning the prediction of wave set-up. As wave set-up and broken wave energy dissipation are closely related (Bonneton, 2007), this result demonstrates that the model gives a realistic description of the energy dissipation.

Concerning the wave shape, Fig. 5b,c shows that the wave skewness and asymmetry are well described before breaking for the 3 grid sizes, but that the discrepancies increase in the surf zone. The wave skewness is still relatively well predicted after breaking, even if a slight underestimation of this parameter is generally observed. Larger discrepancies between experimental and numerical data can be observed for the asymmetry in the surf zone. The model predicts a too large increase of *As* in the first stages of breaking. It corresponds to the steepening of the fronts following the switch from S–GN to NSW equations, and therefore to the shock development. Once the

breaker is fully-developed, the predicted asymmetry stays almost constant, while the asymmetry computed from the experimental data keeps increasing progressively. As expected, the value of *As* increases for decreasing spatial resolution. It is important to keep in mind that the inaccuracies observed in term of asymmetry of the breaking wave front are not specific to our model, but result from the description of breaking wave fronts as shocks by the NSW equations. The choice of δ_x is therefore crucial to obtain a good order of magnitude for the wave asymmetry in the surf zone. As the grid size determines the length of the numerical roller (represented as a shock), the model abilities could probably be improved by relating δ_x to the physical length of the roller, which can be seen as roughly proportional to the characteristic water depth. The use of a variable grid size with δ_x proportional to the characteristic depth could then lead to a better prediction of the left-right asymmetry by the model.

4.1.2. Ting and Kirby (1994)'s experiment

In this section the numerical model is applied to reproduce the laboratory experiments performed by Ting and Kirby (1994) for spilling breakers. Cnoidal waves were generated in the horizontal part of a flume ($h_0 = 0.4$ m) and were propagating over a 1:35 sloping beach. The wave period was $T = 2.0$ s and the incident wave height $H = 0.125$ m. For this experiment, non-synchronized time series of surface elevations and mean characteristic levels (crest, trough and mean water levels) are available at 21 locations in the shoaling and surf zones. For the simulation, the grid size of the mesh is $\delta_x = 0.05$ m and the time step is $\delta_t = 0.01$ s.

Fig. 6 compares the time series of free-surface elevations at different locations, in the shoaling and breaking zone. The main discrepancies are found in the vicinity of the breaking point, where the wave height is underestimated, but the overall agreement improves significantly while propagating shoreward.

Fig. 7a shows the spatial variations of the crest and trough elevations, as well as the variation of the mean water level for the

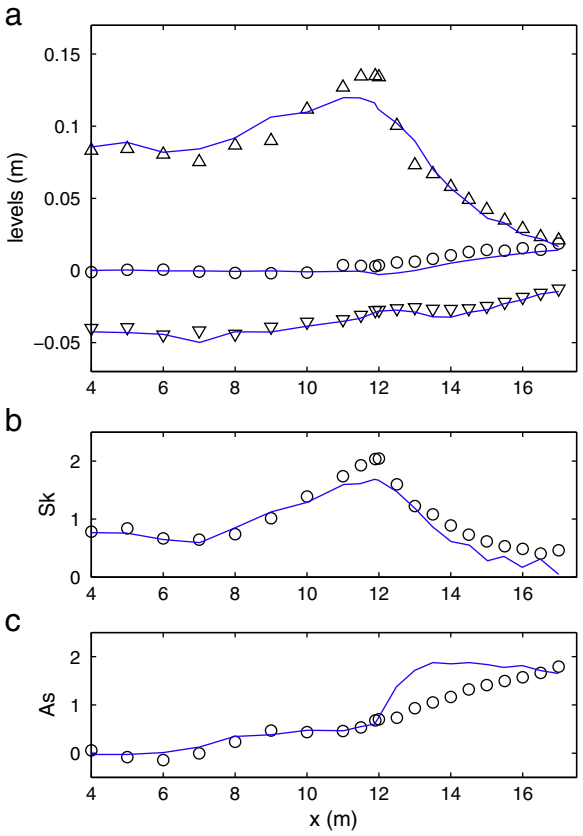

Fig. 7. Spatial evolution of computed (lines) and experimental data (symbols) for Ting and Kirby (1994) spilling breaking experiment. (a) ○: spatial evolution of the mean water level; ▽: trough elevation relative to MWL; △: crest elevation relative to MWL. (b) Wave skewness. (c) Wave asymmetry.

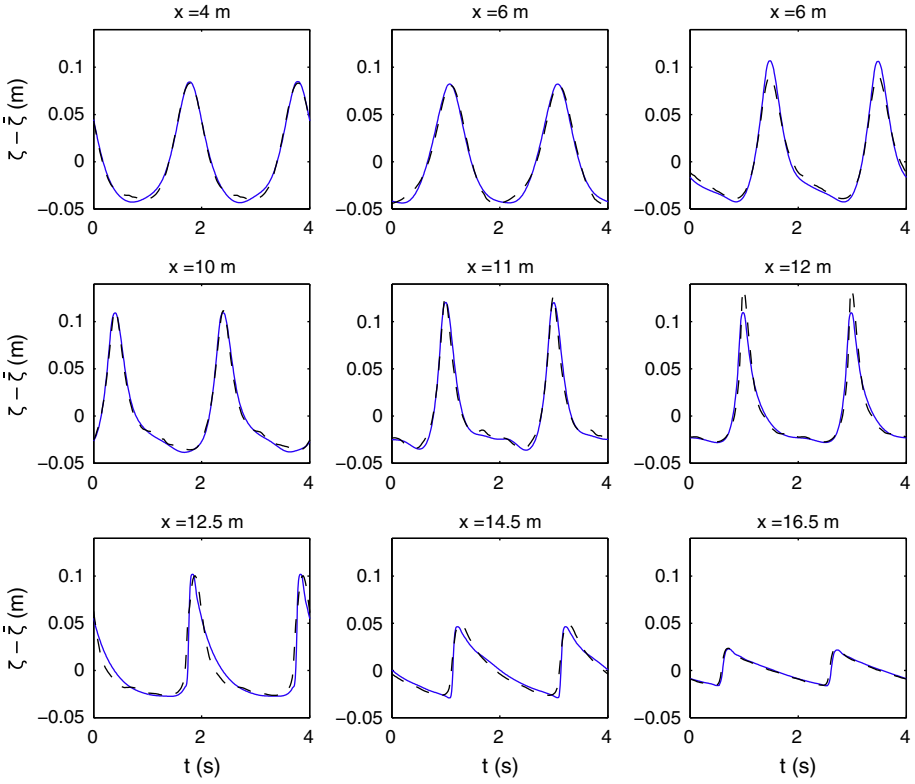

Fig. 6. Comparisons of computed (solid lines) and measured (dashed lines) time series of free-surface elevations for Ting and Kirby experiment at different locations.

experimental and the numerical data. It shows that wave breaking occurs slightly too early in our simulation, explaining part of the wave height underestimation at breaking. It can also be observed that our model tends to underestimate the energy dissipation in the first stages of breaking, leading to a too mild decrease of the wave height in the transition zone. However, it must be noted that the wave height decay rate is well-reproduced in the ISZ ($x \gtrsim 13.5$ m). The discrepancies observed in the transition zone were expected, since the representation of surf zone waves as shocks is *a priori* only accurate when the waves resemble bore-like waves, i.e. in the ISZ. However, previous studies using hybrid models showed that the inaccuracies observed in the first stages of breaking were not affecting significantly the overall predictions of the model (e.g., Tonelli and Petti, 2009, 2010). Finally, we can see in this figure that the set-up prediction is relatively low in most of the surf zone, but that the discrepancies get smaller when the waves propagate shoreward. Similar underestimations of the set-up were obtained with other BT models (see for instance Cienfuegos et al., 2010; Lynett, 2006; Tonelli and Petti, 2010).

Fig. 7b and c presents the spatial evolution of the asymmetry and the skewness, computed from the experimental and numerical time series of free-surface elevation (see Eqs. (11) and (12)). The overall variations of the wave skewness during the onshore propagation are well-reproduced by the model. *Sk* is accurately predicted before breaking, and reaches its maximum at the breaking point. The wave skewness is underestimated in the surf zone, but follows a trend similar to experimental one. Concerning the description of wave asymmetry, the same characteristics as in Section 4.1.1 are observed. Before breaking, a very good agreement between numerical and experimental data is observed. The increase of the skewness at the initiation of breaking is then too steep, leading to significant discrepancies in the surf zone. These discrepancies reduce then gradually while the waves propagate shoreward.

Table 1
Wave heights and non-linear parameters (H/h_0) for the 3 experiments carried out by Hsiao and Lin (2010).

	h_0 (m)	H/h_0
Type 1	0.20	0.35
Type 2	0.22	0.29
Type 3	0.256	0.23

4.2. Solitary wave transformation over a sloping beach (Synolakis, 1987)

In this test case, we assess the ability of our model to describe wave breaking and shoreline motions. It is based on laboratory experiments carried out by Synolakis (1987) for an incident solitary wave of relative amplitude $a_0/h_0 = 0.28$ ($h_0 = 0.3$ m) propagating and breaking over a planar beach with a slope 1:19.85. For this experiment, spatial snapshots at different times are available. The simulations are performed using the grid size $\delta_x = 0.025$ m, and $\delta_t = 0.008$ s. Moreover, a friction term was introduced for this simulation (friction coefficient $f = 0.004$).

The comparisons between measured and computed waves are presented in Fig. 8. We can see that the overall agreement is very good during shoaling, breaking, run-up and run-down. Moreover the model is able to describe the formation and breaking of a backwash bore, which is a particularly demanding test for most of Boussinesq-type models since it involves a broken bore propagating backward.

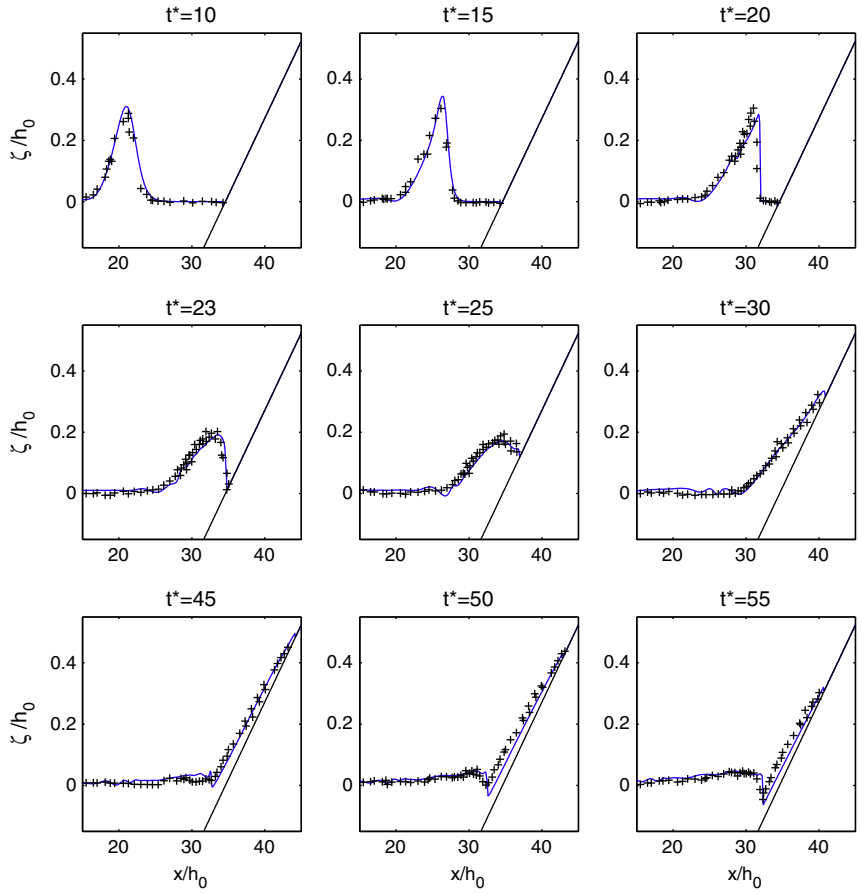

Fig. 8. Comparisons of model predictions (lines) and experimental snapshots (+) at different times for a breaking solitary wave with non-dimensional initial incident amplitude $a_0/h_0 = 0.28$, on a 1:20 plane beach (Synolakis, 1987). $t^* = t(g/h_0)^{1/2}$.

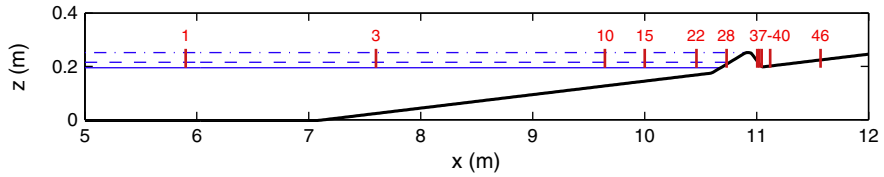

Fig. 9. Schematic view of the experimental set-up in Hsiao and Lin (2010). Vertical lines: location of the wave gauges (WG). Horizontal lines: water levels at rest for the three types of solitary waves described in Table 1.

4.3. Solitary waves overtopping a seawall (Hsiao and Lin, 2010)

We investigate here the ability of our model to describe the complex transformations of solitary waves overtopping a seawall. We consider experiments carried out by Hsiao and Lin (2010) in a 22 *m* long wave flume located in the Tainan Hydraulic Laboratory, National Cheug Kung University, Taiwan. During this experiment, three types of solitary waves were generated. Their characteristics are described in Table 1 (see Fig. 9 for the visualization of the water depth at rest for the 3 cases). In the first case, the solitary wave was breaking on the sloping beach before reaching the wall. In the second case, the solitary wave was breaking on the seawall whereas for case 3 the wave was overtopping directly the seawall without any prior breaking and subsequently collapsing behind the seawall. Hsiao and Lin compared the experimental data with predictions with the volume of fluid (VOF) type model COBRAS (Lin and Liu, 1998), based on Reynolds-Averaged Navier–Stokes equations with $k-\varepsilon$ turbulent closure. They found a very good agreement between experimental data and model predictions, for all stages of wave transformations. This test case will allow us to evaluate the degree of accuracy reachable using a depth-averaged model only.

For our simulations, we choose $\delta_t = 0.007$ s and $\delta_x = 0.02$ m. A quadratic friction term is introduced, with a coefficient $f = 0.01$. As we assume the dispersive effects not to be significant shoreward of the seawall, we decided to suppress them in this entire region. This also prevents the potential development of numerical instabilities at the multiple boundaries between land and water in this case.

Comparisons between the measured and numerical time series of free-surface elevations at the wave gauges are presented in Fig. 10 for the three types of solitary waves. A very good agreement is obtained

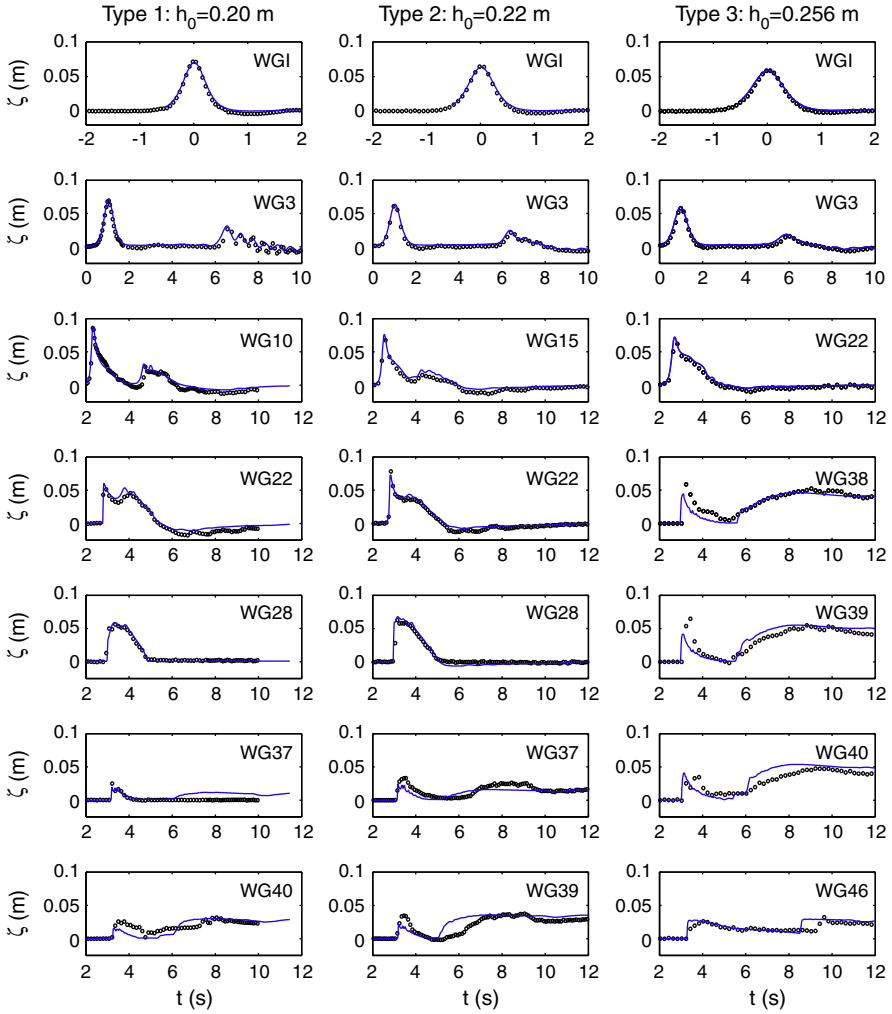

Fig. 10. Comparison between experimental (○) and numerical (plain lines) time series of free-surface elevation for the 3 types of solitary waves described in Table 1 (Hsiao and Lin, 2010).

for the wave gauges located seaward from the wall (see Fig. 10, wave gauges (WG) 1–22) for all the cases. The run-up over the sloping part of the seawall is also well-reproduced (WG28). A part of the wave is reflected over the wall, resulting in the development of an undulated bore propagating seaward for the types 1 and 2. This phenomenon is well described by the model, which highlights its good dispersive properties. The model predictions are a bit less accurate at the wave gauges located just behind the wall. Indeed, if the arrival time of the overtopping wave front is well predicted by the model, its height is generally underpredicted (see WG37–40, for $2<t<5$ *s*). Discrepancies are more important for Type 3. This can be explained by the highly turbulent behaviour of the wave collapsing behind the wall, which cannot be reproduced by our model. A better agreement is observed at the WG46, located further away from the wall. Discrepancies between numerical and experimental data become then more significant for $t>5$ *s* (WG37–46). It corresponds to the run-down of the overtopped water, followed by a new run-up phase after reflection on the seawall.

On the whole, our model gives similar results to those predicted by the more advanced COBRAS model presented in Hsiao and Lin (2010) in terms of time-evolution of the free surface during the first stages of wave overtopping (shoreward propagation). Discrepancies between numerical and experimental data increase during the run-down/run-up phases: these parts of wave evolution are significantly better predicted by the COBRAS model. However, it is important to note that the predicted water depths behind the wall tend to be similar to the experimental ones at the end of the measurements, suggesting a good prediction of the amount of overtopped water.

4.4. Periodic waves breaking over a bar (Beji and Battjes, 1993)

Wave transformations over a bar involve a number of complex processes such as non-linear shoaling, amplification of bound harmonics, and eventually initiation and termination of breaking, with the release of the higher harmonics. A good prediction of these transformations is therefore a challenging test case for the numerical models. In Chazel et al. (2010), our model was successfully applied to the description of non-breaking wave propagation over a submerged bar, allowing for a precise evaluation of its dispersive properties. In the present test case, wave breaking occurs on the top of the bar. We aim at investigating the ability of our model to predict wave-breaking initiation, termination and subsequent transformations after passing the bar.

Beji and Battjes (1993) conducted a series of flume experiments concerning the propagation of regular waves (1 Hz and 0.4 Hz) over a submerged trapezoidal bar, corresponding to either non-breaking, spilling breaking or plunging breaking waves. The bathymetry is presented in Fig. 11: the water depth varies from $h_0=0.4$ m in the deeper region to 0.1 m over the top of the bar. In this section, we focus on the long wave plunging case ($f=0.4$ Hz) as described in Beji and Battjes (1993). Eight wave gauges were deployed, numbered from 1 to 8 in Fig. 11. Experimental and predicted surface elevation time series are compared in Fig. 12. Fig. 13 presents the spatial variations of the significant wave height, computed as four times the standard deviation of the surface elevation, the wave skewness and the wave asymmetry.

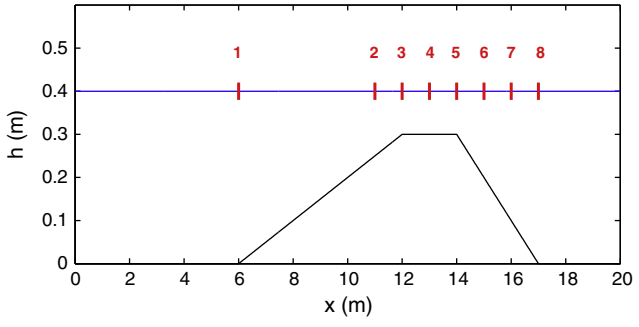

Fig. 11. Schematic view of the experimental set-up in Beji and Battjes (1993). Vertical lines: location of the wave gauges (WG).

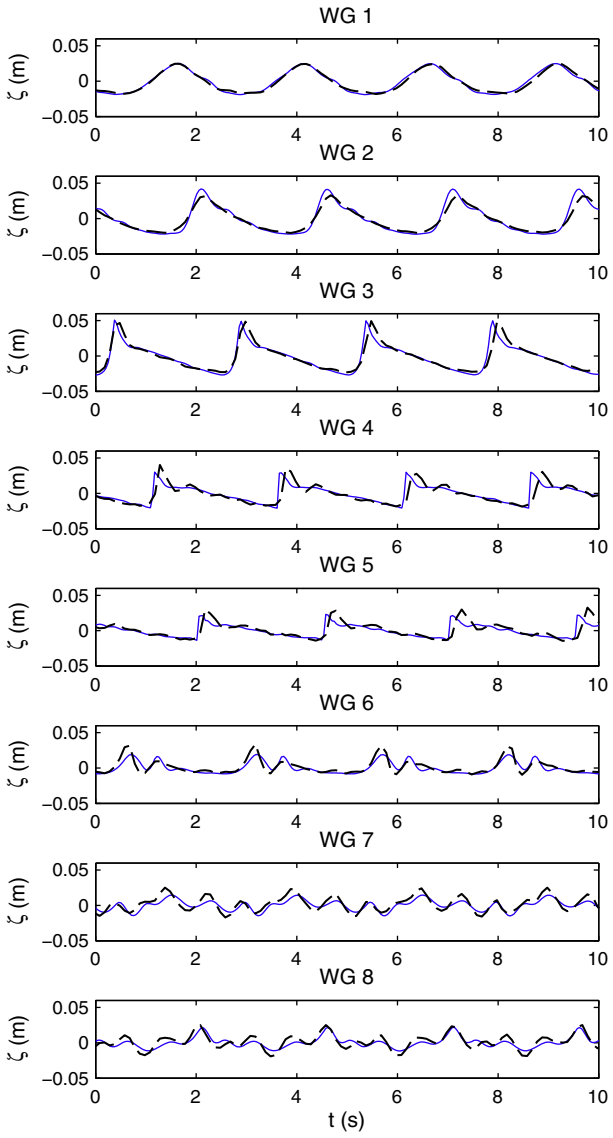

Fig. 12. Comparisons of predicted (plain lines) and measured free-surface elevation time series (dashed lines) at different locations for periodic waves propagating over a bar (Beji and Battjes, 1993: long waves, plunging case).

The wave shape is well-reproduced during the shoaling phase (see Fig. 12, Wave Gauge 2), until the onset of breaking (WG3). This result is illustrated in the Fig. 13b and c, which show a good agreement between the experimental and numerical wave shape parameters at 11 and 12 m. A good agreement is then observed during breaking on the top of the bar, in particular in term of wave height decay (see Fig. 12, WG4–5 and Fig. 13a, $x=12$–14 m). After the bar, the breaking stops and the wave decomposes itself into several smaller amplitude waves, which are in phase with the experimental data and of similar wave length (see Fig. 12, WG6–8). An underestimation of the amplitude is observed at this stage (see also Fig. 13a, $x>14$ m), which seems to indicate that the switch back to S–GN equations happened slightly too late. However, we still have an overall good agreement, indicating that our methodology for the termination of breaking seems adequate, and that the switch from NSW to S–GN

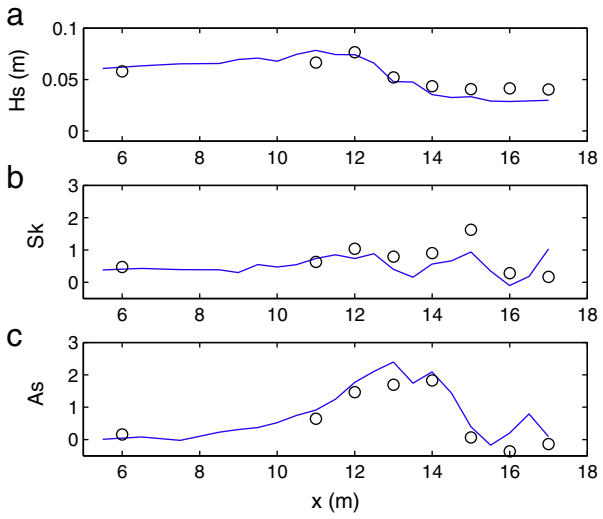

Fig. 13. Spatial evolution of predicted (plain lines) and measured (symbols) wave characteristics for the plunging breaking case of Beji and Battjes (1993)'s experiments. (a) Significative wave height H_s. (b) Wave skewness *Sk*. (c) Wave asymmetry *As*.

equations after the bar gives a good description of the physical processes. It is noteworthy that, to our knowledge, our study is the first one presenting comparisons of experimental and numerical free-surface elevation time series for wave gauges located after the bar for the plunging case of the Beji and Battjes (1993)'s experiments.

Finally, we can see that our model underestimates the wave skewness in the breaking zone above the bar but also after the bar (see Fig. 13b), whereas an overall good agreement is observed concerning the prediction of the wave asymmetry (see Fig. 13c).

4.5. Transition from undular to purely breaking bore

In shallow-water regions, dispersive effects can become significant and affect tsunami wave transformations. Depending on the complex balance between non-linear effects, dispersive effects and energy dissipation due to wave breaking, tsunami wave fronts can evolve into a large range of bore types, from purely undular to purely breaking bore (Grue et al., 2008; Yasuda, 2010). A good prediction of tsunami wave front transformations in shallow water is therefore needed for a better understanding of tsunami run-up and impact on coastal structures. However, previous numerical studies concerning bore dynamics using depth-averaged approaches have been devoted to either purely broken bores using NSW models (e.g., Brocchini and Dodd, 2008), or undular bores using BT models (Soares-Frazão and Zech, 2002; Wei et al., 1995). A model able to reproduce the different bore shapes, as well as the transition from one type of bore to another is required.

Experimentally, it has been showed that the Froude number Fr_1 controls the bore shape as well as the transition from one kind of bore to another (see Section 3.2). Two main transitions are observed at $Fr_1 = Fr_a$ and Fr_b ($Fr_a < Fr_b$). Non-breaking undular bores are observed for $Fr_1 < Fr_a$ (e.g., $Fr_a = 1.3$ in Chanson (2008)). For $Fr_a < Fr_1 < Fr_b$ an undular bore is still developing but the front wave is broken, whereas for $Fr_1 > Fr_b$, a purely breaking bore is observed ($Fr_b = 1.45 - 1.5$ in Chanson (2008)).

In this test case, we assess the ability of our numerical model to reproduce bore dynamics for a large range of Froude numbers. At $t = 0$, we consider initial steps over a flat bottom defined by

$$\begin{cases} h(x,0) = \frac{1}{2}(h_2 - h_1)(1 - tan(x//)) + h_1 \\ u(x,0) = \frac{1}{2}(u_2 - u_1)(1 - tan(x//)) + u_1, \end{cases} \quad (13)$$

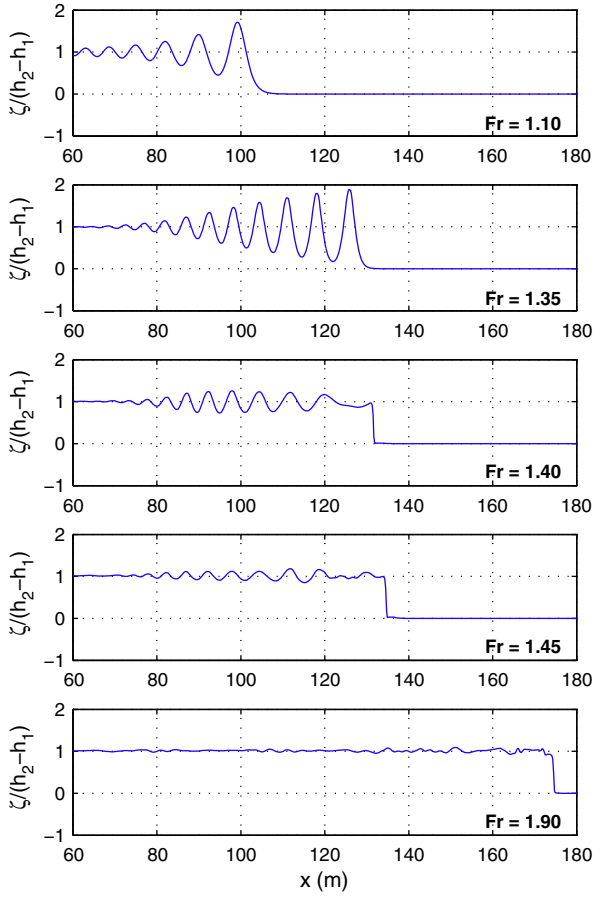

Fig. 14. Normalized free-surface profiles at $t = 30$ s of hydraulic bores with Froude numbers varying from 1.10 to 1.90.

corresponding to Froude numbers varying from 1.10 to 1.90. h_1 and h_2 are the water depth in front and behind the bore, u_1 and u_2 are the corresponding depth-averaged velocities. We set $u_1 = 0$ (water initially at rest), $h_1 = 1$ m and $/ = 2$ m. For each Froude number h_2 and u_2 are deduced from the mass and momentum conservation across the bore. Fig. 14 shows the bore shapes at $t = 30$ s for the different Froude numbers. For $Fr_1 < 1.40$, the initial step evolves into an undular jump (see experimental validation in Tissier et al. (2011) for the undular case). It can be observed that, in agreement with experimental studies, the secondary wave wavelength decreases with increasing Froude number, while the amplitude increases. For $Fr_1 = 1.40$, a wave train is formed but the first wave is broken. Although the first wave seems too damped in comparison with the experimental results, the overall shape at the transition is well-reproduced (see the bore pictures from Treske (1994) for $Fr_1 = 1.35$). It is also in agreement with experiments by Chanson (2008), who observed a flattening of the free-surface elevation for intermediate Froude numbers. For higher Froude numbers, we obtain a strongly breaking bore. It can be observed that some disturbances occur behind the breaking fronts. Their physical relevance still needs to be explored. We observe that our S–GN model is able to reproduce accurately the main features of different bore types, which is a challenging test case for the numerical models. Moreover, the Froude number for the transitions are close to the typical values observed experimentally (see Chanson, 2008; Favre, 1935; Treske, 1994).

5. Conclusion

In this paper, a new approach to handle wave breaking within the framework of hybrid fully non-linear BT models is presented. The

model has been developed as an extension of the well-validated NSW shock-capturing code SURF-WB (Marche et al., 2007), using hybrid finite volume/finite-difference schemes (Bonneton et al., 2011b).

The modeling strategy for wave breaking is based on the splitting of S–GN equations between a hyperbolic part corresponding to the NSWE and a dispersive term. When the wave is ready to break, we switch locally to the NSWE by skipping the dispersive step, such as broken wave fronts can be described as shocks. Energy dissipation due to wave breaking is then predicted by the shock theory, and do not require to be parametrized. The characterization of wave fronts at each time step is easily performed through the study of local energy dissipation. Combined with simple criteria for the initiation and termination of breaking, we obtain an efficient treatment of wave breaking and broken waves propagation without any complex algorithm to follow the waves. Our method has been extensively validated with laboratory data. The ability of our model to reproduce regular wave transformation over slopping beaches has been thoroughly investigated. Application of the model to several cases of overtopping over a seawall and to a case of wave propagation over a bar allowed us to evaluate the model ability to describe wave transformation over complex bathymetries. Finally, promising tests concerning hydraulic bore dynamics were performed, showing that the model is able to reproduce the transitions from undular to purely breaking bores. The study of bore dynamics is a particularly challenging test case since it results from the complex balance between non-linearities, dispersive effects and energy dissipation due to wave breaking.

Work is in progress concerning the 2DH extension of the model. The splitting method used in this model, initially presented in Bonneton et al. (2011b), can be easily extended to 2DH. Its implementation is in progress. The new 2DH S–GN code could be a powerful tool to study the generation of wave-induced circulations and macro-vortices, which are mainly controlled by alongshore variations in breaking wave energy dissipation (Bonneton et al., 2010; Peregrine, 1998).

Acknowledgments

The authors would like to thank Prof. Shih-Chun Hsiao and Ting-Chieh Lin, as well as Prof. Serdar Beji and Prof. Jurjen A. Battjes for providing the experimental data. The authors would like to acknowledge the ANR-funded project MISEEVA, which funded M. Tissier's PhD thesis, and the scientific support of Dr. Rodrigo Pedreros. The authors would also like to acknowledge additional financial and scientific support of the French INSU—CNRS (Institut National des Sciences de l'Univers—Centre National de la Recherche Scientifique) program IDAO ("Interactions et Dynamique de l'Atmosphère et de l'Océan"), as well as the ANR-funded project MathOcean (ANR-09-BLAN-0301-01).

References

Alvarez-Samaniego, B., Lannes, D., 2008. Large time existence for 3D water-waves and asymptotics. Invent. Math. 171, 485–541.
Audusse, E., Bouchut, F., Bristeau, M., Klein, R., Perthame, B., 2004. A fast and stable well-balanced scheme with hydrostatic reconstruction for shallow water flows. SIAM Journal on Scientific Computing 25, 2050–2065.
Beji, S., Battjes, J.A., 1993. Experimental investigation of wave propagation over a bar. Coastal Engineering 19, 151–162.
Berthon, C., Marche, F., 2008. A positive preserving high order VFRoe scheme for shallow water equations: a class of relaxation schemes. SIAM Journal on Scientific Computing 30, 2587–2612.
Berthon, C., Marche, F., Turpault, R., 2011. An efficient scheme on wet/dry transitions for shallow water equations with friction. Computer and Fluids 48.
Bjørkavåg, M., Kalisch, H., 2011. Wave breaking in Boussinesq models for undular bores. Physics Letters A 375, 1570–1578.
Bonneton, P., 2007. Modelling of periodic wave transformation in the inner surf zone. Ocean Engineering 34, 1459–1471.
Bonneton, P., Bruneau, N., Marche, F., Castelle, B., 2010. Large-scale vorticity generation due to dissipating waves in the surf zone. Discrete and Continuous Dynamical Systems—Series B 13, 729–738.
Bonneton, P., Barthelemy, E., Chazel, F., Cienfuegos, R., Lannes, D., Marche, F., Tissier, M., 2011a. Recent advances in Serre-Green Naghdi modelling for wave transformation, breaking and runup processes. European Journal of Mechanics—B/Fluids 30, 589–597.
Bonneton, P., Chazel, F., Lannes, D., Marche, F., Tissier, M., 2011b. A splitting approach for the fully nonlinear and weakly dispersive Green–Naghdi model. Journal of Computational Physics 230, 1479–1498.
Briganti, R., Brocchini, M., Bernetti, R., 2004. An operator-splitting approach for Boussinesq-type equations. GIMC 2004, XV Congresso Italiano di Meccanica Computazionale–AIMETA.
Brocchini, M., Dodd, N., 2008. Nonlinear shallow water equation modeling for coastal engineering. Journal of Waterway, Port, Coastal, and Ocean Engineering 134, 104–120.
Bruno, D., Serio, F.D., Mossa, M., 2009. The FUNWAVE model application and its validation using laboratory data. Coastal Engineering 56, 773–787.
Bühler, O., 2000. On the vorticity transport due to dissipating or breaking waves in shallow-water flow. Journal of Fluid Mechanics 407, 235–263.
Carter, J.D., Cienfuegos, R., 2011. The kinematics and stability of solitary and cnoidal wave solutions of the Serre equations. European Journal of Mechanics - B/Fluids 30, 259–268.
Chanson, H., 2008. Turbulence in positive surges and tidal bores. effects of bed roughness and adverse bed slopes. Hydraulic Model Report No. CH68/08 Div. of Civil Engineering, The University of Queensland, Brisbane, Australia. 121 pages.
Chazel, F., Lannes, D., Marche, F., 2010. Numerical simulation of strongly nonlinear and dispersive waves using a Green–Naghdi model. Journal of Scientific Computing 1–12.
Cienfuegos, R., Barthélemy, E., Bonneton, P., 2006. A fourth-order compact finite volume scheme for fully nonlinear and weakly dispersive Boussinesq-type equations. Part I: model development and analysis. International Journal for Numerical Methods in Fluids 51, 1217–1253.
Cienfuegos, R., Barthélemy, E., Bonneton, P., 2010. Wave-breaking model for Boussinesq-type equations including roller effects in the mass conservation equation. Journal of Waterway, Port, Coastal, and Ocean Engineering 136, 10–26.
Cox, D.T., 1995. Experimental and numerical modelling of surf zone hydrodynamics. Ph.D. thesis. University of Delaware, Newark, Del.
Duncan, J.H., 1981. An experimental investigation of breaking waves produced by a towed hydrofoil. Proceedings of the Royal Society of London. Series A 377, 331–348.
Elgar, S., Gallagher, E.L., Guza, R.T., 2001. Nearshore sandbar migration. Journal of Geophysical Research 106 (C6), 11623–11627.
Erduran, K.S., 2007. Further application of hybrid solution to another form of Boussinesq equations and comparisons. International Journal for Numerical Methods in Fluids 53, 827–849.
Erduran, K.S., Ilic, S., Kutija, V., 2005. Hybrid finite-volume finite-difference scheme for the solution of Boussinesq equations. International Journal for Numerical Methods in Fluids 49, 1213–1232.
Favre, H., 1935. Etude théorique et expérimentale des ondes de translation dans les canaux découverts. Dunod, Paris.
Grasso, F., Michallet, H., Barthélemy, E., 2011. Sediment transport associated with morphological beach changes forced by irregular asymmetric, skewed waves. Journal of Geophysical Research 116.
Green, A.E., Naghdi, P.M., 1976. A derivation of equations for wave propagation in water of variable depth. Journal of Fluid Mechanics 78, 237–246.
Grue, J., Pelinovsky, E.N., Fructus, D., Talipova, T., Kharif, C., 2008. Formation of undular bores and solitary waves in the Strait of Malacca caused by the 26 December 2004 Indian Ocean tsunami. Journal of Geophysical Research C: Oceans 113.
Haller, M.C., Catalán, P.A., 2010. Remote sensing of wave roller lengths in the laboratory. Journal of Geophysical Research 114.
Hsiao, S.C., Lin, T.C., 2010. Tsunami-like solitary waves impinging and overtopping an impermeable seawall: experiment and RANS modeling. Coastal Engineering 57, 1–18.
Kennedy, A.B., Chen, Q., Kirby, J.T., Dalrymple, R.A., 2000. Boussinesq modeling of wave transformation, breaking and run-up. I: one dimension. ASCE Journal of Waterway, Port, Coastal and Ocean Engineering 126 (1), 48–56.
Kirby, J.T., Wei, G., Chen, Q., Kennedy, A.B., Dalrymple, R.A., 1998. FUNWAVE 1.0. Fully nonlinear Boussinesq wave model. Documentation and user's manual. Technical Report CACR-98-06Center for Applied Coastal Research, Department of Civil and Environmental Engineering, University of Delaware.
Kobayashi, N., Silva, G.D., Watson, K., 1989. Wave transformation and swash oscillation on gentle and steep slopes. Journal of Geophysical Research 94, 951–966.
Lannes, D., Bonneton, P., 2009. Derivation of asymptotic two-dimensional time-dependent equations for surface water wave propagation. Physics of Fluids 21.
Lin, P., Liu, P.L.F., 1998. A numerical study of breaking waves in the surf zone. Journal of Fluid Mechanics 359, 239–264.
Lynett, P.J., 2006. Nearshore wave modeling with high-order Boussinesq-type equations. Journal of Waterway, Port, Coastal and Ocean Engineering 132.
Madsen, P.A., Sørensen, O.R., Schäffer, H.A., 1997. Surf zone dynamics simulated by a Boussinesq type model. Part I. Model description and cross-shore motion of regular waves. Coastal Engineering 32, 255–287.
Marche, F., Bonneton, P., Fabrie, P., Seguin, N., 2007. Evaluation of well-balanced bore-capturing schemes for 2D wetting and drying processes. International Journal for Numerical Methods in Fluids 53, 867–894.
Miles, J., Salmon, R., 1985. Weakly dispersive nonlinear gravity waves. Journal of Fluid Mechanics 157, 519–531.
Nwogu, O., 1993. Alternative form of Boussinesq equations for nearshore wave propagation. Journal of Waterway, Port, Coastal and Ocean Engineering 119, 618–638.
Okamoto, T., Basco, D., 2006. The relative trough Froude number for initiation of wave breaking: theory, experiments and numerical model confirmation. Coastal Engineering 53, 675–690.

Orszaghova, J., Borthwick, A.G., Taylor, P.H., 2012. From the paddle to the beach—a Boussinesq shallow water numerical wave tank based on Madsen and Sørensen's equations. Journal of Computational Physics 231, 328–344.
Peregrine, D.H., 1983. Breaking waves on beaches. Annual Review of Fluid Mechanics 15, 149–178.
Peregrine, D., 1998. Surf zone currents. Theoretical and Computational Fluid Dynamics 10, 295–309.
Roelvink, D., Reniers, A., van Dongeren, A., van Thiel de Vries, J., McCall, R., Lescinski, J., 2009. Modelling storm impacts on beaches, dunes and barrier islands. Coastal Engineering 56, 1133–1152.
Ruessink, B.G., Van Den Berg, T.J.J., Van Rijn, L.C., 2009. Modeling sediment transport beneath skewed asymmetric waves above a plane bed. Journal of Geophysical Research C: Oceans 114.
Schäffer, H.A., Madsen, P.A., Deigaard, R., 1993. A Boussinesq model for waves breaking in shallow water. Coastal Engineering 20, 185–202.
Serre, F., 1953. Contribution à l'étude des écoulements permanents et variables dans les canaux. Houille Blanche 8, 374–388.
Shi, F., Kirby, J.T., Harris, J.C., Geiman, J.D., Grilli, S.T., 2012. A high-order adaptive time-stepping TVD solver for Boussinesq modeling of breaking waves and coastal inundation. Ocean Modelling 43–44, 36–51.
Shiach, J.B., Mingham, C.G., 2009. A temporally second-order accurate Godunov-type scheme for solving the extended Boussinesq equations. Coastal Engineering 56, 32–45.
Smith, J.A., 2006. Wave-current interactions in finite depth. Journal of Physical Oceanography 36.
Soares-Frazão, S., Guinot, V., 2008. A second-order semi-implicit hybrid scheme for one-dimensional Boussinesq-type waves in rectangular channels. International Journal for Numerical Methods in Fluids 58, 237–261.
Soares-Frazão, S., Zech, Y., 2002. Undular bores and secondary waves—experiments and hybrid finite-volume modeling. Journal of Hydraulic Research, International Association of Hydraulic Engineering and Research (IAHR) 40, 33–43.
Stocker, J.J., 1957. Water Waves—The Mathematical Theory With Applications. Interscience Publishers, Inc.
Synolakis, C.E., 1987. The runup of solitary waves. Journal of Fluid Mechanics 185, 523–545.
Ting, F.C., Kirby, J.T., 1994. Observation of undertow and turbulence in a laboratory surf zone. Coastal Engineering 24, 51–80.
Tissier, M., Bonneton, P., Marche, F., Chazel, F., Lannes, D., 2011. Nearshore dynamics of tsunami-like undular bores using a fully nonlinear Boussinesq model. Journal of Coastal Research SI 64.
Tonelli, M., Petti, M., 2009. Hybrid finite volume—finite difference scheme for 2DH improved Boussinesq equations. Coastal Engineering 56, 609–620.
Tonelli, M., Petti, M., 2010. Finite volume scheme for the solution of 2D extended Boussinesq equations in the surf zone. Ocean Engineering 37, 567–582.
Tonelli, M., Petti, M., 2012. Shock-capturing Boussinesq model for irregular wave propagation. Coastal Engineering 61, 8–19.
Treske, A., 1994. Undular bores (Favre-waves) in open channels—experimental studies. Journal of Hydraulic Research 32, 355–370.
Wei, G., Kirby, J.T., Grilli, S.T., Subramanya, R., 1995. A fully nonlinear Boussinesq model for surface waves. Part 1. Highly nonlinear unsteady waves. Journal of Fluid Mechanics 294, 71–92.
Weston, B.P., Taylor, P.H., Borthwick, A.G.L., Hunt, A.C., 2003. Godunov-type Boussinesq modelling of extreme wave run-up. Shallow Flows: Research Presented at the International Symposium on Shallow Flows, Delft, Netherlands, pp. 98–403.
Yasuda, H., 2010. One-dimensional study on propagation of tsunami wave in river channels. Journal of Hydraulic Engineering ASCE 136.
Zelt, J.A., 1991. The run-up of nonbreaking and breaking solitary waves. Coastal Engineering 15, 205–246.
Zijlema, M., Stelling, G.S., Smit, P., 2011. SWASH: An operational public domain code for simulating wave fields and rapidly varied flows in coastal waters. Coastal Engineering 58, 992–1012.